

Serveur Académique Lausannois SERVAL serval.unil.ch

Author Manuscript

Faculty of Biology and Medicine Publication

This paper has been peer-reviewed but does not include the final publisher proof-corrections or journal pagination.

Published in final edited form as:

Title: Morphine withdrawal recruits lateral habenula cytokine signaling to reduce synaptic excitation and sociability.

Authors: Valentinova K, Tchenio A, Trusel M, Clerke JA, Lalive AL, Tzanoulinou S, Matera A, Moutkine I, Maroteaux L, Paolicelli RC, Volterra A, Bellone C, Mameli M

Journal: Nature neuroscience

Year: 2019 Jul

Issue: 22

Volume: 7

Pages: 1053-1056

DOI: [10.1038/s41593-019-0421-4](https://doi.org/10.1038/s41593-019-0421-4)

In the absence of a copyright statement, users should assume that standard copyright protection applies, unless the article contains an explicit statement to the contrary. In case of doubt, contact the journal publisher to verify the copyright status of an article.

1 **Morphine withdrawal recruits lateral habenula cytokine signaling to**
2 **reduce synaptic excitation and sociability**

3

4 Kristina Valentinova^{1,4,6}, Anna Tchenio^{1,6}, Massimo Trusel¹, Joseph A.
5 Clerke¹, Arnaud L. Lalive¹, Stamatina Tzanoulidou³, Alessandro Matera⁵,
6 Imane Moutkine², Luc Maroteaux², Rosa C. Paolicelli⁵, Andrea Volterra¹,
7 Camilla Bellone³ and Manuel Mameli^{1,2*}

8

9 ¹ The Department of Fundamental Neuroscience, The University of Lausanne
10 1005 Lausanne, Switzerland.

11 ² Inserm, UMR-S 839, 75005 Paris, France.

12 ³ Department of Basic Neuroscience, The University of Geneva, Switzerland.

13 ⁴ Department of Physiology, The University of Bern, Bern, Switzerland.

14 ⁵ Department of Physiology, The University of Lausanne 1005 Lausanne,
15 Switzerland.

16 ⁶These authors equally contributed to the work.

17

18

19 To whom correspondence should be addressed:

20 Manuel Mameli, PhD

21 ORCID ID: 0000-0002-0570-6964

22 The Department of Fundamental Neuroscience, The University of Lausanne
23 1005 Lausanne, Switzerland.

24 Email manuel.mameli@unil.ch

25

26

27

28

29

30

31

32

33

34

35 **Abstract**

36 **The lateral habenula (LHb) encodes aversive stimuli contributing to**
37 **negative emotional states during drug withdrawal. Here, we report that**
38 **morphine withdrawal (MORwd) in mice leads to microglia adaptations** 39
40 **and diminishes glutamatergic transmission onto raphe-projecting LHb**
41 **neurons. Chemogenetic inhibition of this circuit promotes MORwd-like**
42 **social deficits. MORwd-driven synaptic plasticity and reduced sociability**
43 **require TNF α release and neuronal TNF-Receptor-1 activation. Hence,**
44 **habenular cytokines control synaptic and behavioral adaptations during**
45 **drug withdrawal.**

46 Opiate withdrawal produces negative states including low mood and reduced
47 sociability, contributing to relapse during drug abstinence^{1,2}. Dysfunction of
48 the lateral habenula (LHb) – a nucleus controlling monoaminergic systems
49 and processing aversive stimuli – underlies depressive symptoms typical of
50 drug withdrawal³, yet how opiates affect the LHb remains poorly known^{4,5}.

51
52 We subjected mice to naloxone-precipitated MORwd to examine its
53 repercussions on glutamatergic synapses onto LHb neurons¹. Indeed,
54 aberrant LHb excitatory transmission underlies negative symptoms in rodent
55 models of depression and addiction³. Spontaneous excitatory postsynaptic
56 current (sEPSC) amplitudes, but not frequencies, were reduced only in LHb
57 neurons located in the medial aspect (^{Med}LHb; lateral LHb, ^{Lat}LHb;
58 Supplementary Fig. 1a–b). Accordingly, MORwd diminished AMPAR:NMDAR
59 ratios solely in ^{Med}LHb (Fig. 1a and Supplementary Fig. 1c) without affecting
60 neurotransmitter release assessed by trains of synaptic stimulation
61 (Supplementary Fig. 1d). Recordings obtained 1 hour after the last MOR
62 injection (without naloxone) yielded saline-comparable AMPAR:NMDAR
63 ratios. In contrast, spontaneous MORwd decreased AMPAR:NMDAR ratios in
64 the ^{Med}LHb up to 30 days after the last MOR injection (Supplementary Fig. 65
65 1e).
66

67 To assess whether MORwd affects AMPAR conductance or number, we used
68 peak-scaled non-stationary fluctuation analysis of ^{Med}LHb-recorded sEPSCs⁶.
69 While single-channel conductance remained unaffected in MORwd slices, the
70 number of channels opened at the peak positively correlated with amplitude
71 values (Supplementary Fig. 1f). MORwd failed to alter AMPAR-EPSC
72 rectification (Supplementary Fig. 1g), whereas it reduced glutamate uncaging-
73 evoked AMPAR:NMDAR ratios, yielding a decrease only in absolute AMPAR
74 currents (Supplementary Fig. 1h). This suggests that MORwd reduces, in a
75 territory-specific fashion, the number of AMPARs without affecting their
76 biophysical properties, NMDARs or presynaptic glutamate release.

77

78 MORwd-evoked plasticity occurs onto ^{Med}LHb neurons, which innervate
79 downstream structures including the raphe nucleus and the ventral tegmental
80 area (VTA)⁷. MORwd diminished AMPAR:NMDAR ratios solely in retrobeads-
81 labeled Raphe– but not VTA–projecting LHb neurons (LHb_{Raphe} and LHb_{VTA})
82 (Fig. 1b, c) pointing to its specificity for discrete habenular circuits.

83

84 Which induction mechanism gates MORwd-driven plasticity onto ^{Med}LHb
85 neurons? Inflammatory responses and glial cell activation emerge during drug
86 withdrawal⁸. Indeed, spontaneous MORwd drives microglia adaptations and 87
87 pro-inflammatory cytokine release (i.e. tumor necrosis factor- α (TNF α))⁹.

88 Notably, cocaine also leads to reduced microglia arborization along with
89 TNF α -dependent AMPAR internalization, partly underlying drug-mediated
90 behavioral adaptations⁸. We found that, within the ^{Med}LHb, MORwd i. reduced
91 microglial markers including Iba1 and CD68 and ii. diminished microglial cell
92 volume (Fig. 2a–d). In parallel, naloxone- and spontaneous MORwd
93 increased habenular TNF α immunolabeling (Fig. 2e and Supplementary Fig.
94 2a–d). Altogether, these findings support the engagement of inflammatory
95 responses and cytokine signaling within the LHb during MORwd.

96

97 We then reasoned that if MORwd promotes TNF α release, artificially
98 increasing its levels should prove sufficient to recapitulate MORwd-driven 99
99 synaptic plasticity. Incubating LHb-containing slices from saline-injected mice

100 with exogenous TNF α reduced AMPAR:NMDAR ratios in the ^{Med}LHb. This 101
effect was absent in ^{Lat}LHb, and occluded by naloxone and spontaneous
102 MORwd (Fig. 2f–g and Supplementary Fig. 3a). TNF α release may arise from
103 microglial Toll-Like Receptor 4 (TLR-4) signaling¹⁰. Systemically activating
104 TLR-4 with the agonist MPLA in MOR-treated mice, instead of naloxone,
105 mimicked MORwd plasticity (Supplementary Fig. 3b). Moreover, MPLA
106 application in slices from MOR-treated animals reduced AMPAR currents in
107 ^{Med}LHb, but not ^{Lat}LHb (Supplementary Fig. 3c–d). MPLA-driven EPSCs
108 reduction did not occur in presence of a dominant negative peptide, which
109 blocks the soluble form of TNF α (XENP1595; Supplementary Fig. 3e)⁸.
110 Furthermore, MORwd occluded MPLA-driven synaptic depression
111 (Supplementary Fig. 3c) and systemic injection of XENP1595 prevented
112 MORwd-induced plasticity (Supplementary Fig. 3f). Altogether, this supports
i. 113 TLR-4 expression within the LHb (See Allen Brain Atlas), *ii.* its effect on
114 AMPARs via TNF α signaling, and *iii.* the necessity and sufficiency of TNF α for
115 MORwd-driven reduction of LHb glutamatergic transmission.

116

117 TNF α triggers its central effects partly through TNF receptor-type-1 (TNF-
118 R1)¹¹. We employed TNF-R1^{fl/fl} mice to Cre-dependently knock-down TNF-R1
119 expression in LHb neurons (Fig. 3a–c). After viral injection, AAV_{Cre}-TNF-R1^{fl/fl}
120 mice failed to show MORwd-driven AMPAR:NMDAR ratio reduction compared
121 to AAV_{Control}-infused mice (Fig. 3d). This highlights the necessity of neuronal
122 TNF-R1 for MORwd-driven depression of synaptic AMPARs in LHb.

123

124 MORwd drives negative symptoms among which social detachment¹.
125 Similarly, LHb dysfunction contributes to the negative states emerging in
126 addiction, although its implications for sociability remains poorly addressed.
127 We examined the contribution of the LHb-to-Raphe pathway, the locus of
128 MORwd plasticity, for social behavior. We employed an intersectional
129 chemogenetic approach to reduce the efficiency of the LHb-to-Raphe
130 projection. This combined the retrograde expression of cre-recombinase
131 (HSV-Cre, dorsal raphe) with cre-dependent expression of hM4Di (rAAV-
132 hM4Di-mCherry, DREADDi, LHb; Fig. 3e). Reducing LHb-to-Raphe efficiency

133 with clozapine-N-oxide diminished social preference (Fig. 3f), supporting LHb
134 contribution to social behaviors.

135 Next, we recapitulated MORwd-driven reduction in social preference in
136 C57Bl6 mice (Fig. 3g and Supplementary Fig. 4a–d). We then prepared slices
137 from MORwd mice showing low or high sociability scores, and found that
138 ^{Med}LHb AMPAR:NMDAR ratios positively correlated with the social score (Fig.
139 3h). This indicates that reduced synaptic strength in the LHb predicts opiate-
140 WD-driven sociability deficits.

141 Notably, microglia and TNF α signaling also contributes to social behaviors¹².
142 Accordingly, MORwd-driven sociability deficits were absent after cre-
143 dependent LHb TNF-R1 knock-down (Fig. 3i and Supplementary Fig. 4e–i).
144 This genetic intervention did not affect locomotion (Supplementary Fig. 4j).
145

146 We found that MORwd-driven TNF α release requires neuronal TNF-R1 to
147 reduce AMPAR transmission onto raphe-projecting, medially-located, LHb
148 neurons. This ultimately gates MORwd-driven social impairment, a negative
149 symptom typical of opiate withdrawal.

150

151 **T**ogether with sociability deficits, MORwd also leads to anxiety and
152 hyperalgesia¹. Since the contribution of LHb on these two behavioral aspects
153 remains elusive we cannot rule out that MORwd-driven habenular plasticity is
154 specific for withdrawal-mediated sociability defects.

155 The TNF α -TNF-R1 engagement within the LHb represents a previously
156 unidentified mechanism underlying precise cellular and behavioural aspects
of 157 MORwd. Yet this is consistent with the following: *i.* drugs and drug-
158 withdrawal-mediated modulation of AMPAR transmission partly rely on
159 cytokine signaling⁸; *ii.* inhibition of TLR-4 attenuates MORwd symptoms¹³; *iii.*
160 TNF-Rs contribute to social behaviors¹⁴. Notably, in pyramidal neurons of the
161 hippocampus and cortex, TNF α regulates AMPAR surface expression^{15,16}.

162 This phenomenon is opposite at striatal synapses where, similarly to the LHb,
163 TNF α application results in decreased AMPAR transmission⁸. This divergence
164 may arise from different TNF α release dynamics, TNF receptors expression
165 and signaling, or alternatively AMPAR anchoring properties within the LHb.

166 MORwd modifies the morphology of microglia in the LHb. This is, at least
167 partly, consistent with previous findings⁸, yet it remains correlative with
168 respect to TNF α levels. This heightens the need to fill the gap in
169 understanding microglia function and its relationship with TNF α within the
170 habenula. Overall, while pharmacotherapies targeting pro-inflammatory
171 pathways in substance abuse are missing, our data support cytokine
signaling
172 as a cellular pillar for aspects of drug addiction.
173 MORwd-driven TNF α -dependent depression of AMPAR transmission occurs
174 at LHb_{Raphe} neurons. From a circuit standpoint, this may provide an 'anti-
175 social' signal likely through reduced actions onto raphe neuronal populations.
176 This is consistent with the evidence reported here that chemogenetic
177 manipulation of the LHb-to-Raphe projection diminishes sociability. Alongside,
178 dopamine- and serotonin-containing raphe neurons contribute to social
179 behaviors, and medially-located LHb neurons monosynaptically connect to the
180 latter¹⁷⁻¹⁹. Understanding the repercussions of LHb activity onto raphe
181 neuronal subtypes during MORwd remains an important aspect for future
182 investigation.

184

185 In conclusion, our data support the participation of cytokine-mediated
186 plasticity for opiate-evoked negative symptoms, a mechanism by which LHb
187 ultimately contributes to the addiction spiral.

188

189 **Acknowledgements**

190 We thank F.J. Meye and the Mameli Laboratory for comments on the
191 manuscript. This work was supported by funds from the ERC StG Saliensy
192 335333, the SNSF (31003A) to M.M. We thank David Szymkowski for the
193 donation of XENP1595, Georg Kollias and Hiltrud Strubbe for the use and
194 breeding of TNF-R1 mouse line.

195

196 **Author contributions**

197 K.V., A.T. and M.M. performed and analyzed *ex vivo* recordings and behavior.
198 A.L.L and J.A.C. contributed to *ex-vivo* recordings. M.T. I.M. and L.M.

199 performed molecular biology experiments. C.B. and S.T. provided support for
200 behavioral experiments. A.M. and R.C.P. analyzed microglia morphology.
201 A.V. provided conceptual and experimental input related to the TNF α
202 signaling and TNFR1^{fl/fl} mice. K.V. and M.M. conceptualized, designed the
203 study and wrote the manuscript.

204

205 **Competing financial interests**

206 The authors declare no competing financial interests.

207

208

209

210

211

212

213

214

215

216

217

218 **References**

- 219 1. Goeldner, C. *et al.* Impaired emotional-like behavior and serotonergic
220 function during protracted abstinence from chronic morphine. *Biol*
221 *Psychiatry* **69**, 236-244 (2011).
- 222 2. Lutz, P. E. *et al.* Distinct mu, delta, and kappa opioid receptor
223 mechanisms underlie low sociability and depressive-like behaviors
224 during heroin abstinence. *Neuropsychopharmacology* **39**, 2694-2705
225 (2014).
- 226 3. Meye, F. J., Trusel, M., Soiza-Reilly, M. & Mameli, M. Neural circuit
227 adaptations during drug withdrawal - Spotlight on the lateral habenula.
228 *Pharmacol Biochem Behav* **162**, 87-93 (2017).
- 229 4. Margolis, E. B. & Fields, H. L. Mu Opioid Receptor Actions in the Lateral
230 Habenula. *PLoS One* **11**, e0159097 (2016).
- 231 5. Wang, J. *et al.* Inhibition of the lateral habenular CaMKII abolishes
232 naloxone-precipitated conditioned place aversion in morphine-dependent
233 mice. *Neurosci Lett* **653**, 64-70 (2017).
- 234 6. Valentinova, K. & Mameli, M. mGluR-LTD at Excitatory and Inhibitory
235 Synapses in the Lateral Habenula Tunes Neuronal Output. *Cell Rep* **16**,
236 2298-2307 (2016).
- 237 7. Pollak Dorocic, I. *et al.* A whole-brain atlas of inputs to serotonergic
238 neurons of the dorsal and median raphe nuclei. *Neuron* **83**, 663-678
239 (2014).
- 240 8. Lewitus, G. M. *et al.* Microglial TNF- α Suppresses Cocaine-Induced
241 Plasticity and Behavioral Sensitization. *Neuron* **90**, 483-491 (2016).
- 242 9. Campbell, L. A., Avdoshina, V., Rozzi, S. & Mochetti, I. CCL5 and
243 cytokine expression in the rat brain: differential modulation by chronic
244 morphine and morphine withdrawal. *Brain Behav Immun* **34**, 130-140
245 (2013).
- 246 10. Michaud, M. *et al.* Proinflammatory cytokines, aging, and age-related
247 diseases. *J Am Med Dir Assoc* **14**, 877-882 (2013).
- 248 11. Probert, L. TNF and its receptors in the CNS: The essential, the
249 desirable and the deleterious effects. *Neuroscience* **302**, 2-22 (2015).
- 250 12. Nie, X. *et al.* The Innate Immune Receptors TLR2/4 Mediate Repeated
251 Social Defeat Stress-Induced Social Avoidance through Prefrontal
252 Microglial Activation. *Neuron* **99**, 464-479.e7 (2018).
- 253 13. Hutchinson, M. R. *et al.* Proinflammatory cytokines oppose opioid-
254 induced acute and chronic analgesia. *Brain Behav Immun* **22**, 1178-1189
255 (2008).
- 256 14. Patel, A., Siegel, A. & Zalcman, S. S. Lack of aggression and anxiolytic-
257 like behavior in TNF receptor (TNF-R1 and TNF-R2) deficient mice.
258 *Brain Behav Immun* **24**, 1276-1280 (2010).
- 259 15. He, P., Liu, Q., Wu, J. & Shen, Y. Genetic deletion of TNF receptor
260 suppresses excitatory synaptic transmission via reducing AMPA receptor
261 synaptic localization in cortical neurons. *FASEB J* **26**, 334-345 (2012).
- 262 16. Stellwagen, D., Beattie, E. C., Seo, J. Y. & Malenka, R. C. Differential
263 regulation of AMPA receptor and GABA receptor trafficking by tumor
264 necrosis factor-alpha. *J Neurosci* **25**, 3219-3228 (2005).
- 265 17. Kane, M. J. *et al.* Mice genetically depleted of brain serotonin display
266 social impairments, communication deficits and repetitive behaviors:

267 possible relevance to autism. *PLoS One* **7**, e48975 (2012).
268 18. Lecca, S. *et al.* Aversive stimuli drive hypothalamus-to-habenula
269 excitation to promote escape behavior. *Elife* **6**, (2017).
270 19. Matthews, G. A. *et al.* Dorsal Raphe Dopamine Neurons Represent the
271 Experience of Social Isolation. *Cell* **164**, 617-631 (2016).
272
273
274
275
276
277
278
279
280
281

282 **Figure legends**

283 **Figure 1 MORwd-driven projection-specific synaptic depression in LHb.**

284 (a) Naloxone-precipitated MORwd (NP-MORwd) protocol and
285 AMPAR:NMDAR ratios from ^{Lat}LHb (saline+naloxone ($n_{\text{mice/cells}}=7/11$; gray)
286 versus NP-MORwd ($n_{\text{mice/cells}}=8/11$; orange): two-sided t-test, $t_{20}=0.0548$,
287 $P=0.957$) and ^{Med}LHb: (saline+naloxone ($n_{\text{mice/cells}}=7/12$; black) versus NP-
288 MORwd ($n_{\text{mice/cells}}=8/13$; red): two-sided t-test, $t_{23}=2.210$, $*P=0.037$) (b)
289 Retrobeads in Raphe (left) and retrogradely-labeled LHb_{Raphe} neurons (right)
290 images. AMPAR:NMDAR ratios from LHb_{Raphe} neurons (saline+naloxone
291 ($n_{\text{mice/cells}}=5/10$; black) versus NP-MORwd ($n_{\text{mice/cells}}=5/11$, red), two-sided t-
292 test, $t_{19}=3.153$, $**P=0.005$). (c) Same as c but in VTA (saline+naloxone
293 ($n_{\text{mice/cells}}=2/6$; black) versus NP-MORwd ($n_{\text{mice/cells}}=4/7$; red), two-sided t-test,
294 $t_{11}=0.575$, $P=0.577$). Sal, saline; Mor, morphine; Nlx, naloxone; PAG,
295 periaqueductal gray; DG, dentate gyrus; MHb, medial habenula; SNr,
296 substantia nigra pars reticulata. Data are presented as box plots 10-90
297 percentiles with median and scatter.

298

299 **Figure 2 Cytokine signaling in the LHb for MORwd plasticity.**

300 (a) Max-projection of confocal acquisition of LHb of Iba1-positive microglia
301 (left). Max-projection of ^{Med}LHb microglia in saline+naloxone and NP-MORwd
302 mice (top right). 3D reconstruction of Iba1 positive microglia, containing CD68
303 structures in saline+naloxone and NP-MORwd (bottom right). (b) Analysis of
304 Iba1 microglia immunoreactivity in ^{Med}LHb (Saline+naloxone (black)
305 $n_{\text{mice/cells}}=4/366$, NP-MORwd (red) $n_{\text{mice/cells}}=4/328$, two-sided t-test, $t_{692}=3.305$,
306 $***P=0.001$; three independent acquisition sessions). (c, d) Quantitative
307 analysis of microglial cell volume (based on Iba1-immunoreactivity) and
308 CD68-positive structures. Values are normalized to Saline control
309 (Saline+naloxone (black) $n_{\text{mice/cells}}=4/89$, NP-MORwd (red) $n_{\text{mice/cells}}=4/83$; Iba1
310 volume, two-sided t-test, $t_{170}=3.05$, $**P=0.003$; CD68/Iba1 volume, two-sided
311 t-test, $t_{170}=2.65$, $**P=0.008$). Measurements were obtained from independent
312 samples. (e) TNF α (cyan) and DAPI (magenta) immunostaining and
313 normalized TNF α optical density in the LHb (saline+naloxone ($n_{\text{mice}}=7$; 6
314 independent acquisitions/mouse; black) versus NP-MORwd ($n_{\text{mice}}=8$; red; 5

315 independent acquisitions/mouse), two-sided t-test, $t_{13}=2.991$, $*P=0.0104$). (f)
316 Experimental protocol and AMPAR:NMDAR ratios in ^{Lat}LHb without (–) or with
317 (+) exogenous TNF α (saline+naloxone (–) TNF α $n_{mice/cells}=2/9$; $\square\square\square\square$ vs
318 saline+naloxone (+)TNF α $n_{mice/cells}=2/9$; lighter gray \square : two-sided t-test,
319 $t_{14}=0.37$, $P=0.717$). (g) AMPAR:NMDAR ratios without (–) or with (+)
320 exogenous TNF α $\square\square\square\square\square\square\square\square$ from saline+naloxone (black, $n_{mice/cells}=3/10$
321 and gray, $n_{mice/cells}=4/11$) and NP-MORwd ^{Med}LHb slices (red, $n_{mice/cells}=3/10$
322 and pink, $n_{mice/cells}=5/15$) (interaction factor $F_{(1,42)}=4.90$ two-way ANOVA,
323 $*P=0.039$). Data are presented as box plots 10-90 percentiles with median
324 and scatter.

325

326 **Figure 3 TNFR1 requirements for MORwd-driven synaptic and**
327 **behavioural adaptations.**

328 (a) Experimental protocol. (b) Image and (c) quantification of AAV-Cre-
329 infected LHb neurons (magenta) and total LHb neurons (cyan; 3 mice: M1, M2
330 and M3). (d) AMPAR:NMDAR ratios from ^{Med}LHb of: AAV_{Control}-TNF-R1^{fl/fl}
331 (saline+naloxone ($n_{mice/cells}=2/9$; gray) versus NP-MORwd ($n_{mice/cells}=3/14$;
332 red)) or AAV_{Cre}-TNF-R1^{fl/fl} (saline+naloxone ($n_{mice/cells}=4/13$; open gray) versus
333 NP-MORwd ($n_{mice/cells}=3/12$; open pink)) (interaction factor $F_{(1,44)}=4.887$ two-
334 way ANOVA, $*P=0.032$). (e) AAV-Control or AAV-Flex-DREADDi virus
335 injections in the LHb and HSV-Cre virus in the Raphe. (f) Tracking, box and
336 scatter plots of social preference test (SPT) in C57Bl6 mice expressing or not
337 DREADDi in LHb-to-raphe neurons (Control virus (black) versus DREADDi
338 (red), $n_{mice}=8$ /group, $t_{18}=2.271$, $*P=0.043$). (g) Tracking plots of social
339 preference test (SPT) in C57/Bl6 mice. Box/scatter plots showing social
340 preference score (saline+naloxone (black) versus NP-MORwd (red), $n_{mice}=22$
341 /group, $t_{42}=2.559$, $*P=0.014$). Full circles indicate mice used for recordings in
342 h. (h) Correlation of AMPAR:NMDAR ratios and social preference score
343 ($n_{mice/cells}=4/12$; Pearson's $r^2=0.954$; $*P=0.023$). Shaded circles represent
344 single cell, full circles represent average per mouse (mean and sem). (i)
345 Tracking and box/scatter plots of SPT in TNF-R1^{fl/fl} mice (AAV_{Control}:
346 saline+naloxone ($n_{mice}=20$; black), NP-MORwd ($n_{mice}=20$; red), AAV_{Cre}:
347 saline+naloxone (open gray), NP-MORwd (open pink), $n_{mice}=13$ mice/group,

348 interaction factor $F_{(1, 65)} = 7.20$ two-way ANOVA, $**P = 0.009$). S, social
349 stimulus; O, object. Data are presented as box plots 10-90 percentiles with
350 median and scatter.

351

352

353 **Methods**

354 **Animals and morphine treatments.** C57Bl/6J wild-type (male) and 129-
355 Tnfrsf1atm3Gkl (male and female, referred as TNF-R1^{fl/fl}) mice of 4–10 weeks
356 were group-housed (three to five per cage) on a 12:12 h light cycle (lights on
357 at 7 a.m.) with food and water ad libitum. All procedures aimed to fulfill the 3R
358 criterion and were approved by the Veterinary Offices of Vaud (Switzerland;
359 License VD3172). Part of the current study was carried out in the Institut du
360 Fer a Moulin, Paris and experiments were in accordance with the guidelines
361 of the French Agriculture and Forestry Ministry. Morphine withdrawal was
362 either precipitated with naloxone or was induced naturally. For naloxone-
363 precipitated morphine withdrawal, mice were subjected to six-day
364 intraperitoneal (i.p.) morphine (20mg/kg, Cantonal Hospital of Lausanne,
365 CHUV, Switzerland) or saline injections (saline and morphine-treated animals
366 were housed together). On day 6, the last morphine/saline injection was given
367 in a separate cage, thirty minutes after which animals received an i.p. injection
368 of naloxone hydrochloride (2mg/kg, Abcam). Morphine withdrawal
369 dependence symptoms were allowed to develop in the following thirty
370 minutes, after what mice were either sacrificed for *ex vivo* electrophysiological
371 recordings or were subjected to behavioral tests.

372

373 For spontaneous withdrawal, mice were treated with morphine or saline for 6
374 days and were sacrificed for recordings 10-13, 20 or 30 days after the last
375 injection. For recordings in morphine-treated animals not in withdrawal, mice
376 were sacrificed one hour after the last morphine injection on day 6. To assess
377 TNF α involvement in morphine withdrawal plasticity, part of the animals were
378 subjected to an i.p. injection of MPLA (Monophosphoryl Lipid A, 10 μ g, a Toll-
379 like receptor 4 activator dissolved in DMSO and saline) or saline (containing
380 the same amount of DMSO as control)⁸ instead of naloxone thirty minutes
381 after the last morphine injection on day 6. Another portion of the animals
382 received an i.p. injection of a dominant negative peptide blocking the soluble
383 form of TNF α , XENP1595, 30mg/kg, Xencor, US)⁸ one hour prior the last
384 morphine or saline injection on day 6. Thirty minutes after the morphine/saline
385 injection these animals received naloxone and were sacrificed for recordings

386 as described above. No statistical methods were chose to pre-determine
387 sample sizes but our sample sizes are similar to those reported previously⁶.
388

389 **Surgery.** Animals of at least 4 weeks were anesthetized with ketamine (150
390 mg/kg)/xylazine (100 mg/kg) i.p. (Veterinary office University of Lausanne)
391 and were placed on a stereotactic frame (Kopf, Germany). Bilateral injections
392 of 200-400 nl volume were performed through a glass needle, at a rate of
393 approximately 100 nl min⁻¹. The injection pipette was withdrawn from the
394 brain 10 min after the infusion. Retrobeads (Lumafluor) were infused into the
395 dorsal raphe nucleus (A-P:-3.5; M-L:0;D-V:-3.8 mm) or ventral tegmental area
396 (A-P:-2.4; M-L:±0.65;D-V:-4.9 mm) of C57Bl6 mice. 129-Tnfrsf1atm3Gki mice
397 were injected with either rAAV2-hSyn-eGFP or rAAV2-hSyn or CMV-Cre-
398 eGFP into the LHb (A-P:-1.35; M-L: ±0.45;D-V:-3.00 mm). In another set of
399 experiments C57Bl6 mice were injected with a herpes simplex virus derived
400 hEF1α-cre vector (MGA Gene delivery technology core, Cambridge, MA,
401 USA) in the raphe nucleus and with rAAV-DJ-EF1α-Flex-hM4D(Gi)-mCherry
402 (Gene vector and virus core, Stanford medicine, CA, USA) in the LHb.
403 Animals were allowed to recover for about 5-7 days after retrobeads injections
404 or 5 weeks after viral infusion before being submitted to morphine/saline
405 treatment. The injection sites were carefully examined for all electrophysiology
406 experiments and only animals with correct injections were used for
407 recordings. Similarly, for behavioral studies only animals with correct injection
408 sites were included in the analysis. Brain slices from mice injected with
409 retrobeads or viruses were directly examined under an epifluorescence
410 microscope.

411

412 **Ex-vivo electrophysiology.** Animals of 5 weeks were anesthetized with
413 ketamine/ xylazine; 150 mg/kg/100 mg/kg i.p. for preparation of LHb-
414 containing brain slices. Slicing was done in bubbled ice- cold 95% O2/5%
415 CO2-equilibrated solution containing (in mM): choline chloride 110; glucose
416 25; NaHCO3 25; MgCl2 7; ascorbic acid 11.6; sodium pyruvate 3.1; KCl 2.5;
417 NaH2PO4 1.25; CaCl2 0.5. Coronal slices (250 µm) were prepared and
418 transferred for 10 min to warmed solution (34 °C) of identical composition,
419 before they were stored at ~22 °C in 95% O2/5% CO2-equilibrated artificial

420 cerebrospinal fluid (ACSF) containing (in mM): NaCl 124; NaHCO₃ 26.2;
421 glucose 11; KCl 2.5; CaCl₂ 2.5; MgCl₂ 1.3; NaH₂PO₄ 1. Recordings (flow
422 rate of 2.5 ml/min) were made under an Olympus-BX51 microscope
423 (Olympus) at 32 °C. Patch-clamp experiments were performed using
424 borosilicate glass pipettes (2.7–4 MΩ; Phymep, France). Currents were
425 amplified, filtered at 5 kHz and digitized at 20 kHz (Multiclamp 200B;
426 Molecular Devices, USA). Data were acquired using Igor Pro with NIDAQ
427 tools (Wavemetrics, USA). Access resistance was monitored by a step of –4
428 mV (0.1 Hz). Experiments were discarded if the access resistance increased
429 more than 20%. All recordings were made in voltage-clamp configuration.
430 Spontaneous EPSCs were recorded either in the lateral or in the medial
431 territory of the LHb at –60 mV in presence of picrotoxin (100 μM, Abcam) and
432 APV (50 μM, Abcam). The internal solution contained (in mM): CsCl 130;
433 NaCl 4; MgCl₂ 2; EGTA 1.1; HEPES 5; Na₂ATP 2; sodium creatine-
434 phosphate 5; Na₃GTP 0.6; spermine 0.1. The liquid junction potential was –3
435 mV and was not compensated. For AMPAR:NMDAR ratios EPSCs were
436 evoked through glass electrodes placed ~200 μm from the recording site
437 using AMPI ISO-Flex stimulator. A mixture of AMPA and NMDA currents were
438 evoked at +40 mV (in presence of picrotoxin). The two components were
439 pharmacologically isolated by adding APV in the recording solution and by
440 subsequent identification of the individual currents via digital subtraction. For
441 glutamate uncaging experiments MNI-glutamate (4-methoxy-7-nitroindoliny-
442 caged L-glutamate 500μM, Tocris) was added to the recording solution.
443 Uncaging was obtained via a single-path photolysis head (Prairie
444 Technologies) connected to a solid-state laser (Rapp Optoelectronics,
445 Germany; 405 nm, duration 1 ms, diameter 3–5μm, 250-300μm from soma).
446 AMPAR:NMDAR ratios in uncaging experiments were calculated as follows:
447 AMPA-EPSC at –60 mV/NMDA-EPSCs at +40 mV and the individual
448 components were identified as previously described, using the late
449 component of the EPSC at 30 ms after the onset. Rectification index was
450 computed by recording AMPA-EPSC at –70 and +40 mV and was calculated
451 as follows: (AMPA-EPSC at –70/AMPA-EPSC at +40)/1.75. To assess
452 presynaptic release properties, trains of AMPAR-EPSCs were evoked using

453 extracellular stimulating electrode (5 pulses at 5Hz, 10Hz and 20Hz). The
454 amplitudes of EPSCs trains were normalized to the amplitude of the first
455 pulse. When indicated recordings were performed from retrogradely labeled
456 and fluorescently identified Lhb neurons. Some experiments were performed
457 in Lhb-containing slices incubated for minimum one hour with exogenous
458 TNF α (100ng/ml). To test the effect of MPLA on AMPAR transmission,
459 neurons were patched either in the lateral or the medial territory of the Lhb
460 and EPSCs were evoked with extracellular stimulation. Following a ten-minute
461 baseline, MPLA (1 μ g/ml) was added to the recording solution and EPSCs
462 were recorded minimum 40 minutes after. Some experiments were performed
463 in presence of the TNF α -dominant negative peptide μ 6mg/1ml;
464 XENP1595, Xencor, US) in the recording solution.

465

466 **Non stationary fluctuation analysis.**

467 A peak-scaled nonstationary fluctuation analysis (NSFA) was performed on
468 sEPSCs (# of events, 70–250) (Synaptosoft, USA). sEPSCs were selected
469 by: fast rise time alignment, stable baseline holding current, and the absence
470 of spurious fluctuations during the sEPSCs decay. The variance–amplitude
471 relationship of sEPSC decay was plotted and fitted with the equation
472 $\sigma^2 = iI - I^2/N + \sigma_b^2$ (where i is the mean single-channel AMPA current, I is the
473 mean current, N is the number of channels activated at the peak, $N = \text{mean}$
474 $\text{amplitude}/i$; and σ^2 is the baseline variance). i was estimated as the slope of
475 the linear fit of the first portion of the parabola of the fitted sEPSC decay. The
476 goodness-of-fit was assessed with a least-squares algorithm. The unitary
477 current was converted in conductance based on the reversal potential of
478 evoked EPSCs (0 mV) and the holding potential (–60 mV). Conductance and
479 average EPSC amplitude, mean rise time, mean decay time, access
480 resistance, or background noise variance had no correlation ($p > 0.4$).

481

482 **Histology and immunofluorescence.** Mice were injected daily with
483 saline/morphine (20mg/kg, i.p.) for 6 days. Some mice were left to develop
484 spontaneous withdrawal, while others received naloxone (2mg/kg, i.p.)
485 injection 30 min after the last saline/morphine injection on day 6. After 10-13

486 days of spontaneous withdrawal or 30 min after naloxone injection mice were
487 anesthetized and perfused with cold 4% paraformaldehyde (PFA) in PBS
488 (phosphate-buffered saline). The brains were extracted, post-fixed in 4% PFA
489 in PBS, and incubated in 30% sucrose in PBS until they sank. 30 μ m slices
490 were cut at the cryostat, and stored in PBS containing 0.02% NaN₃ for future
491 analysis. For the immunofluorescence, the slices were incubated 2h in
492 blocking buffer (5% NGS, 0.3% Triton-X in PBS) and then 24h at 4°C with the
493 primary antibody solution (mouse anti-TNF α antibody, ab1793, Abcam, 1:100
494 in blocking buffer⁸). After extensive rinses, the secondary antibody was
495 applied (goat anti-mouse IgG-conjugated Alexa 488, Invitrogen, 1:400 in
496 blocking buffer, 24h at 4°C). The slices were then incubated in a 1:400 DAPI
497 solution in PBS, extensively rinsed, mounted on glass slides with Pro-Long
498 Gold Antifade Reagent (Invitrogen) and coverslipped. Images were acquired
499 with an epifluorescent microscope with a 20x objective (AxioVision, Zeiss)
500 using the same parameters for all the samples. The images were analyzed
501 and processed with ImageJ software. Optical density was measured on the
502 whole LHb area, and normalized on the neighboring thalamus [LHb-
503 Thal/(LHb+Thal)]. 3-6 slices distributed in the rostrocaudal axis were analyzed
504 per each animal (8 morphine, 7 saline).

505

506 **Microglia analysis**

507 Mice were anesthetized and perfused with cold 4% paraformaldehyde (PFA)
508 in PBS (phosphate-buffered saline). The brains were extracted, post-fixed in
509 4% PFA in PBS, and incubated in 30% sucrose in PBS until they sank. 30 μ m
510 slices were cut at the cryostat, and stored in PBS containing 0.02% NaN₃ for
511 future analysis. Brain sections were permeabilized at room temperature (RT)
512 in 0.5% Triton X-100 (Sigma) for 1 hr RT, followed by 1 hr RT blocking in 2%
513 BSA 0.5% Triton X-100 and overnight incubation with primary antibody (Iba1
514 1:1000, Wako Chemicals, Cat. No. 019-19741 and CD68 1:400, Bio-Rad Cat.
515 No. MCA1957⁸) at 4°C. Upon washing, sections were incubated 2 hr RT with
516 Alexa-fluorophore-conjugated secondary antibodies (Invitrogen), and
517 counterstained with DAPI (Invitrogen).

518 Confocal microscopy was performed with a TCS-SP5 (Leica) Laser Scanning
519 System, by using a 20X dry objective and images were processed and

520 analyzed by Fiji Software or Imaris Software (Bitplane, Switzerland), as
521 appropriate. Imaris was used for 3D rendering of confocal images for
522 quantification of volumes.

523 For density analysis, for each acquisition, the DAPI channel was max-
524 projected and the medial and lateral portions of the lateral habenula were
525 manually drawn as region of interest. Then, stacks ranging from 15 to 20 μ m in
526 thickness, with z-step size of 1 μ m, were processed as follows: Iba1 and DAPI
527 channels were thresholded in Fiji and multiplied to each other for each stack,
528 with the image calculator function. The resulting thresholded stack was max-
529 projected and the microglia nuclei were counted with Analyze Particle
530 function.

531 For cell soma size and Iba1 intensity, each acquisition was max-projected and
532 the contour of cell somata in the medial portion of the lateral habenula were
533 manually drawn based on the Iba1 immunoreactivity, and analyzed per size in
534 μ m² and intensity.

535 3D imaging analysis was performed by Imaris applying recorded algorithms
536 (fixed thresholds for signal intensity) to all the images of the same experiment,
537 in order to produce unbiased signal quantification. In each experiment, one
538 brain slice per animal (n=4) per each group was acquired. The microglial cell
539 volume and the volume of phagocytic structures were reconstructed based on
540 the absolute intensity of Iba1 and CD68 signals, respectively. The volume of
541 CD68 was then normalized for the Iba1 volume, to take in account the cell
542 size.

543

544 **Behavior.**

545 **Social preference test.** A three-chambered social preference test was used,
546 consisting in a rectangular Plexiglas arena (60 × 40 × 22 cm) (Ugo Basile,
547 Varese, Italy) divided into three chambers. The walls of the center chamber
548 had doors to allow free access to all compartments. The luminosity was
549 around 10 lux. Thirty minutes after naloxone injection each mouse was placed
550 in the arena for a habituation period of 10 min and was allowed to freely
551 explore the whole empty arena. The social preference test was performed
552 immediately after the end of the habituation: two enclosures with vertical bars
553 were placed in the middle of the two lateral compartments, while the central

554 chamber remained empty. One enclosure was empty (serving as an
555 inanimate object) whereas the other contained a social stimulus (unfamiliar
556 juvenile mouse 25 ± 1 days old). The enclosures allowed visual, auditory,
557 olfactory and tactile contact between the experimental mice and the social
558 stimuli mice. The juvenile mice in the enclosures were habituated to the
559 apparatus and the enclosures for 3 days before the experiment and each one
560 of them served as a social stimulus for no more than 2 experimental mice (at
561 least 6 weeks old). The test lasted 10 minutes where experimental mice were
562 allowed to freely explore the apparatus and the enclosures. The position of
563 the empty and juvenile-containing enclosures alternated and was
564 counterbalanced for each trial to avoid any bias effects. Every session was
565 video-tracked and recorded using Ethovision XT (Noldus, Wageningen, the
566 Netherlands) or AnyMaze (Stoelting, Ireland), which provided an automated
567 recording of the entries and time spent in the compartments, the distance
568 moved and the velocity. The time spent in each chamber was assessed and
569 then used to determine the preference score for the social compartment as
570 compared to the object compartment ($\text{social}/(\text{social} + \text{object})$). The arena was
571 cleaned with 1% acetic acid solution and dried between trials.

572

573 **Analysis and statistics.** Animals were randomly assigned to experimental
574 groups. Compiled data are always reported and represented as whisker box
575 plots (whisker top/bottom represent 90/10th percentile, box top/bottom
576 represent 75/25th percentile and median) or mean \pm SEM, with single data
577 points plotted (single cell for electrophysiology and single animal for
578 behavioral experiments). Animals or data points were not excluded unless
579 stated and normality test was applied. Data collection and analysis were not
580 performed blind to the conditions of the experiments. When applicable,
581 statistical tests were paired or unpaired t-test and one-way or two-way
582 ANOVA. Significance for correlations was obtained applying Pearson's
583 estimates. Testing was always performed two-tailed with $\alpha = 0.05$. More
584 information on the methods and analysis can be found in the Life Science
585 Reporting Summary.

586

587

588 **Data availability statement**

589 The data sets generated during and/or analyzed during the current study are
590 available from the corresponding author on reasonable request.

591

592

593

594

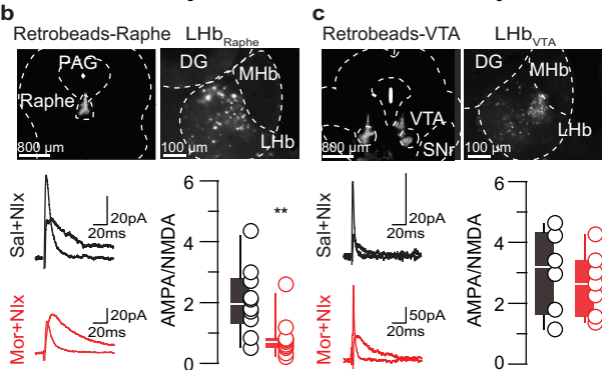
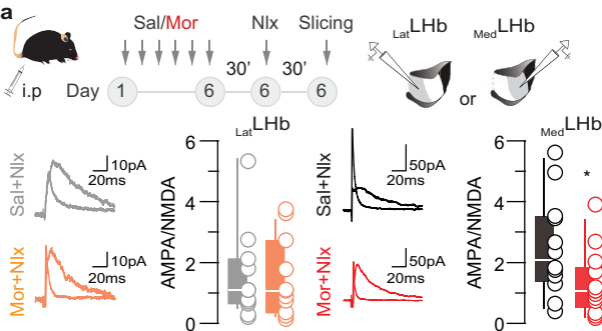


Fig 1., Valentinova, Tchenio et al.

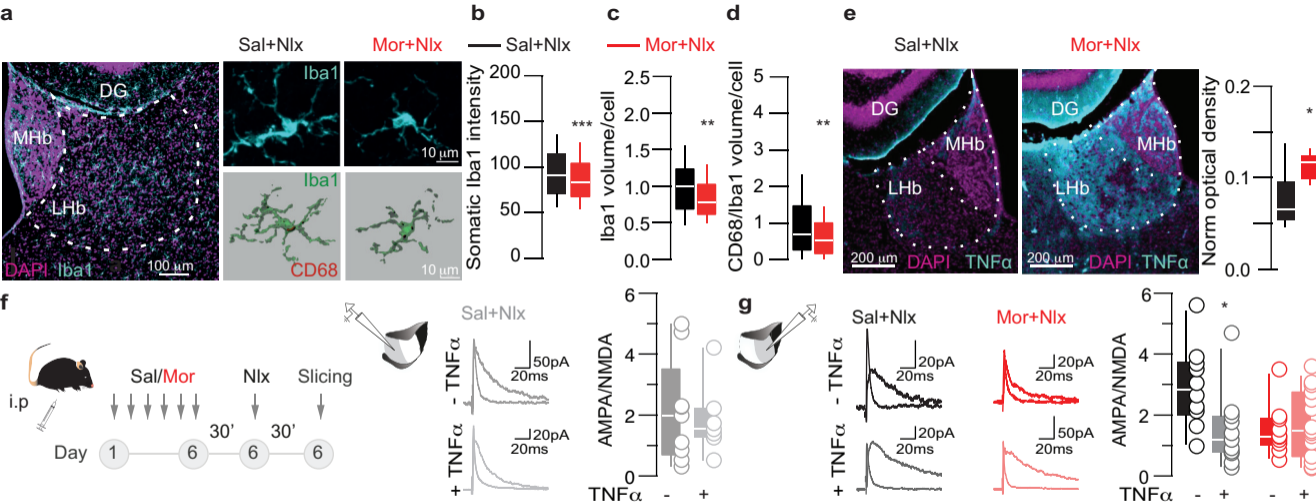


Fig 2., Valentinova, Tchenio et al.

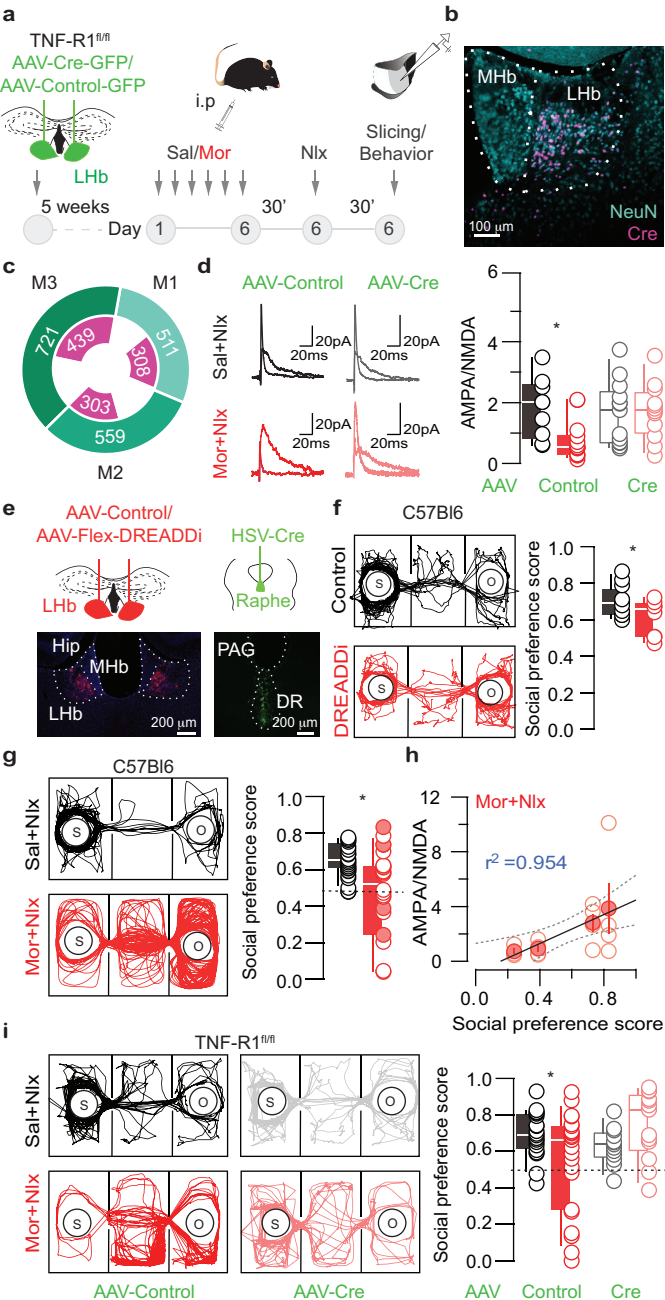


Fig 3., Valentinova, Tchenio et al.